Placenta 121 (2022) 99–108

Contents lists available at ScienceDirect

Placenta

journal homepage: www.elsevier.com/locate/placenta

# Maternal, placental, and fetal distribution of titanium after repeated titanium dioxide nanoparticle inhalation through pregnancy

J.N. D'Errico [a], C. Doherty [b], J.J. Reyes George [a], B. Buckley [a,b], P.A. Stapleton [a,b,*]

[a] Department of Pharmacology and Toxicology, Ernest Mario School of Pharmacy, Rutgers University, 160 Frelinghuysen Rd, Piscataway, NJ, 08854, USA
[b] Environmental and Occupational Health Sciences Institute, 170 Frelinghuysen Rd, Piscataway, NJ, 08854, USA

ARTICLE INFO

*Keywords:*
Titanium dioxide nanoparticles
Placenta
Fetal sex
Intrauterine position
ICP-MS
TEM

ABSTRACT

Epidemiological studies have associated ambient engineered nanomaterials or ultrafine particulate matter ($PM_{0.1}$), collectively referred to as nanoparticles (NPs), with adverse pregnancy outcomes including miscarriage, preterm labor, and fetal growth restriction. Evidence from non-pregnant models demonstrate that NPs can cross the lung air-blood barrier and circulate systemically. Therefore, inhalation of NPs during pregnancy leading to fetoplacental exposure has garnered attention. The purpose of this study was to evaluate the distribution of inhaled titanium dioxide nanoparticles (nano-$TiO_2$) from the maternal lung to maternal and fetal systemic tissues. Pregnant Sprague Dawley rats were administered whole-body exposure to filtered air or of nano-$TiO_2$ aerosols (9.96 ± 0.06 mg/$m^3$) between gestational day (GD) 4 and 19. On GD 20 maternal, placental, and fetal tissues were harvested then digested for ICP-MS analysis to measure concentrations of titanium (Ti). TEM was used to visualize particle internalization by the placental syncytium. The results demonstrate the extrapulmonary distribution of Ti to various maternal organs during pregnancy. Our study found Ti accumulation in the decidua/junctional and labyrinth zones of placentas embedded in all sections of uterine horns. Further, NPs deposited in the placenta, identified by TEM, were found intracellularly within nuclear, endoplasmic reticulum, and vesicle organelles. This study identified the systemic distribution and placental accumulation of Ti after nano-$TiO_2$ aerosol inhalation in a pregnancy model. These findings arouse concerns for poor air quality for pregnant women and possible contributions to adverse pregnancy outcomes.

## 1. Introduction

Ambient particulate matter (PM) with diameters of 0.1 μm (100 nm) or less are considered to be part of the ultrafine fraction of particulate matter ($PM_{0.1}$). Enabled by their small size, $PM_{0.1}$, otherwise recognized as nanoparticles (NPs), can cross biological barriers with considerable ease [1–3]. Over recent years, the global increases in aerosolized particulate matter [4], as well as the rapid development of engineered NPs, raises the potential for inhalation and systemic distribution of NPs across the pulmonary air-blood barrier. Particle translocation from the lung has been demonstrated in real-world human exposures [5,6] and controlled animal studies [7,8].

Pregnancy complications (e.g., miscarriage, fetal growth restriction) associated with PM exposure manifest in both human and animal studies which suggests a link between pulmonary NP exposure and adverse pregnancy outcomes [9–11]. Recent work gives further cause for concern over maternal inhalation of ambient NPs during pregnancy and their distribution [12]. Human placentas collected after delivery show that inhaled NPs can travel to the placenta [12]. Using electron microscopy and energy dispersive X-ray spectroscopy, PM consistent with the morphology, clustering, and chemical construct of $PM_{0.1}$ from combustion-associated processes were found on the fetal side of the placenta after real-world exposure throughout pregnancy [12]. Additional evidence from animal studies reveal that pulmonary exposures to nano-polystyrene [9] or engineered nano-silver [10] led to placental and fetal distribution. Altogether, this evidence supports the theory that NPs inhaled during pregnancy can disseminate through the body, reaching the placenta and fetal tissues. Therefore, consideration is growing for underrepresented individuals, such as pregnant women and their children, who may be more vulnerable to these exposures.

Characterizing absorption or uptake and distribution are critical components to understanding toxicokinetics of NPs that enters the body.

* Corresponding author. Department of Pharmacology and Toxicology, Ernest Mario School of Pharmacy, Environmental and Occupational Health Sciences Institute, Rutgers University, 170 Frelinghuysen Road, Piscataway, NJ, 08854, USA.
*E-mail address:* stapleton@eohsi.rutgers.edu (P.A. Stapleton).

https://doi.org/10.1016/j.placenta.2022.03.008
Received 30 November 2021; Received in revised form 7 February 2022; Accepted 3 March 2022
Available online 12 March 2022

Nose-only exposure to titanium dioxide nanoparticles (nano-$TiO_2$) in healthy male rats identified systemic distribution to the filter organs within 3-h of exposure [7]. During pregnancy, the drastic physiological changes associated with gestation may alter the absorption and distribution to secondary tissues, including 30–40% increase in tidal volume, 45% increase in maternal blood volume, and increased blood perfusion of the uterus, liver, and kidneys [13–15]. Together, this suggests that the maternal reproductive tissues, liver, and kidneys may be key sites of NP distribution and accumulation in a pregnancy model; however, this has not been well characterized in the literature.

The placenta is a transient but critical tissue that embeds into the maternal uterus. Given the increase in blood flow to the uteroplacental tissues during pregnancy, the placenta may be a direct target for NP deposition. Maternal blood bathes the placental syncytium cell layer, a 2 or 3 cell layer thick tissue in a human or rodent, respectively, that separates the maternal and fetal circulations. The syncytium is the most important cell type of the placenta performing the critical functions of: 1) fetal barrier protection, 2) expression of plasma membrane receptors that regulate protein synthesis, 3) production and secretion of peptide hormones (e.g., human chorionic gonadotropin), and 4) transport of substances across to the fetal blood circulation. Chemicals or pollutants such as NPs within maternal blood can directly encounter the syncytium. *In vitro* experiments have shown primary human syncytial cells to internalize and accumulate metallic NPs [16]. Once internalized, NPs mainly distribute to lysosomal vesicles while some remain freely suspended in cytoplasm [17]. Other intracellular consequences include NP-protein aggregation, increased endoplasmic reticulum stress, mitophagy, and increased intracellular ROS [17]. Cellular damage to the placenta may cause serious organ dysfunction. NP-mediated decreases in uterine invasion [18] and increases in uterine vascular resistance [19] have been empirically shown to lead to poor placental perfusion. Additional studies have shown decreased placental growth [20], barrier integrity [21], and hormone secretion [22] after NP exposure. Increased inflammatory cytokine secretion [10] and trophoblast shedding [21] from NP exposure have also been identified, all of which can result in attenuated barrier and nutrient provision for the fetus. While these findings are critical to the field, there are inherent limitations. Studies utilize *in vitro* or *ex vivo* models may apply NP doses significantly higher than physiological transport would permit of NP to elicit effects. Those employing short and direct lung instillation exposure schemes (e.g., single or acute exposure timelines and direct intratracheal instillation) often make for difficult extrapolation to the human population who often experience chronic, lower dose exposures to ambient NPs. Therefore, it is critical to utilize a recurring whole-body exposure scheme throughout pregnancy to evaluate inhaled ambient NP aerosol translocation from the lung to the placenta and syncytium internalization.

Fetal sex plays a major role in the outcomes of placental mediation of maternal stress [23], uptake of xenobiotics [11], and likelihood of developing gestational disorders such as preterm birth [24]. A sex-dependent placental accumulation of metals has been identified, where placentas from male fetuses accumulated higher concentrations of soluble silver (Ag) and titanium (Ti) compared to females [25]. This sexual dimorphism is likely due to the contribution of X- and Y- linked genes leading to differential sex-specific regulatory pathways of the placenta. Another emerging and potentially significant contributor to pregnancy outcomes includes intrauterine positioning of the placenta and fetus [11,26]. We identified differences in fetal weight between uterine horns and specific horn locations after maternal nano-$TiO_2$ inhalation [11]. Therefore, these factors may also play a role in placental uptake of NPs.

Here we employ whole-body inhalation exposure to nano-$TiO_2$ aerosols, a widely used engineered nanomaterial and common surrogate for $PM_{0.1}$ exposures, throughout gestation to simulate environmental or occupational workplace exposures as previously identified [27]. The hypothesis of this study is that nano-$TiO_2$ will translocate from the lungs after maternal inhalation in late-stage pregnancy, Ti will be quantified in all secondary maternal, utero-placental, and fetal tissues, and NPs will be visualized in the syncytium. Furthermore, we expect sex- or intrauterine position- specific Ti accumulation. Our aims were to 1) describe the Ti distribution from the pulmonary space to maternal, placental, and fetal tissues, 2) measure Ti accumulation on the maternal and fetal sides of the placenta by sex and intrauterine position, and 3) visualize intracellular localization of NP within placental syncytium.

## 2. Materials and methods

### 2.1. Nanoparticle Characterization

Nano-$TiO_2$ powder was purchased from Evonik (Aeroxide $TiO_2$, Parsippany, NJ). Using dynamic light scattering (DLS) techniques with a Zetasizer Nano ZS by Malvern, the crystalline composition of the powder was previously determined to be composed of 80% anatase and 20% rutile, primary particle size 21 ± 6.1 nm and surface area 48.08 $mg^2/g$ [28].

### 2.2. Animal model

Time-pregnant Sprague Dawley rats were purchased from Charles River Laboratories (Kingston, NY) on GD 1 or 2 and housed in the Rutgers School of Public Health vivarium on GD 2 or GD 3. Animals were single housed, had *ad libitum* access to food (Purina 508 Rodent Chow) and water, and were given a 24–48-h acclamation period prior to first handling. All procedures were approved by the Institutional Animal Care and Use Committee of Rutgers University.

### 2.3. Whole-body nanoparticle exposure

Between GD 4 and GD 19 animals were administered whole-body exposure to HEPA filtered air or nano-$TiO_2$ aerosols in our custom rodent inhalation facility (IEStechno, Morgantown, WV) [28]. Both the HEPA filtered air control group and nano-$TiO_2$ group had a sample size of 6 dams. Animal exposures occurred for 4 h/day 5 days/week with a total of 12 exposure days during gestation. The concentration of the particle aerosols was confirmed via gravimetric sample collection on a 47-nm PTFE membrane filter and an XP2U microbalance (Mettler Toledo, Switzerland) [29]. The size distribution and concentration of the particles were monitored in real-time by a scanning mobility particle sizer (SMPS, TSI, Shoreview, MN) and a particle counter (General Purpose Water-based Condensation Particle Counter, TSI, Shoreview, MN), respectively. The average aerosolized NP agglomerate size was determined to be 175.91 ± 3.35 nm.

The measured ambient particle concentration within the chamber for the 4-h exposure was set at 10 $mg/m^3$ and measured at 9.96 ± 0.06 $mg/m^3$ (Fig. 1), consistent with our previous work [11,28]. The animals were not exposed for the remaining 20-h of each day. Therefore, the cumulative exposure for the 24-h period is 39.84 $mg/m^3$. When converted to a 24-h time weighted average, pregnant rats would be exposed to an hourly average of 1.66 $mg/m^3$. A population study of preterm birth in Wuhan, China recently reported an ambient hourly $PM_{2.5}$ concentration mean of 84.54 $\mu g/m^3$ in their study population, 20-times greater than the concentrations used on our study [30].

For each individual animal the total lung deposition was calculated using a method previously described [31] with the following equation: D = F * V * C * T, where F is the deposition fraction (10%), V is the minute ventilation based on dam body weight (g), C equals the steady state mass concentration ($mg/m^3$), and T equals the exposure duration (minutes). The average sum of lung burdens for each exposure day considering clearance equated to 194.81 ± 1.89 (Table 1).

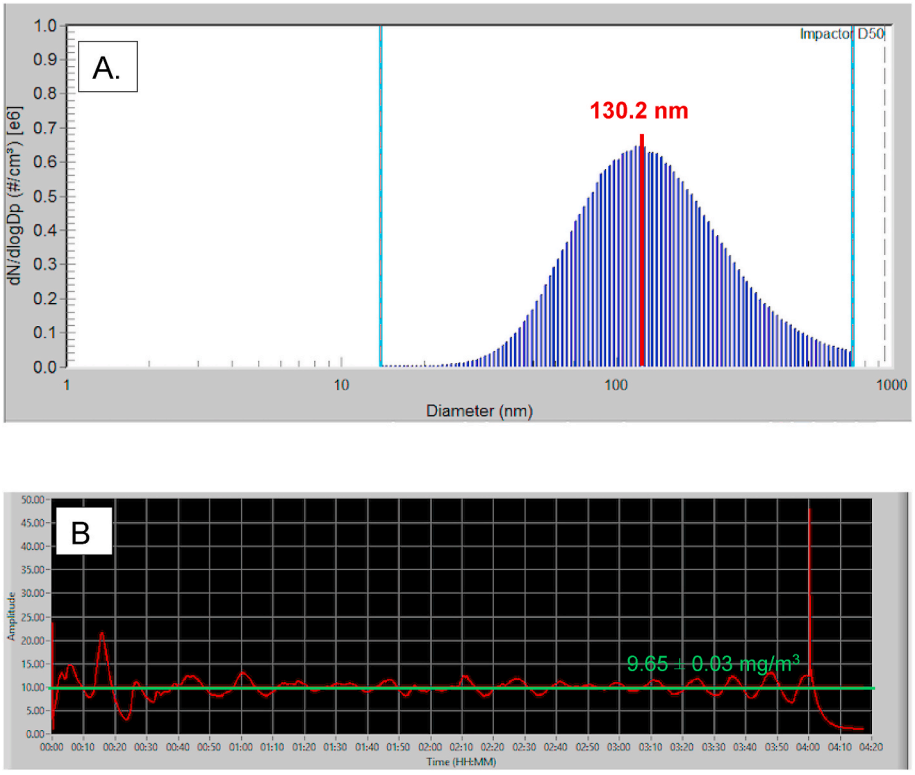


**Fig. 1.** Representations of nanoparticle aerosol characteristics during whole-body animal exposure taken on a single exposure day (4.20.21). **A.** A representative histogram of the particle size distribution measured within the chamber in real-time by a Scanning Mobility Particle Sizer (SMPS). The SMPS determined the median aerosolized particle diameter to be 130.2 nm for this sample of chamber air. **B.** Real-time nanoparticle concentration monitoring within the exposure chamber over the span of a 4-h nano-$TiO_2$ exposure. The overall average chamber particle concentration for this exposure was 9.65 ± 0.03 mg/$m^3$ and the peak amplitude was 48.01 mg/$m^3$.

**Table 1**
Calculated NP lung burden with the following equation: D = F * V * C * T, where F is the deposition fraction (10%), V is the minute ventilation based on dam body weight (g), C equals the steady state mass concentration (mg/$m^3$), and T equals the exposure duration (minutes). Mean ± SEM reported. The average additive sum of lung burdens for each exposure day considering clearance equated to 194.81 ± 1.89 μg.

| Treatment Group | n | Total Deposition (ug) | Daily Deposition Considering Clearance (ug) | Additive Daily Deposition Considering Clearance (ug) |
|---|---|---|---|---|
| Filtered Air Control | 6 | 0 | 0 | 0 |
| Nano-$TiO_2$ Exposed | 6 | 608.79 ± 5.90 | 16.23 ± 0.16 | 194.81 ± 1.89 |

### 2.4. Tissue Collection

At approximately 9:45 a.m. on GD 20 animals were placed under anesthesia with 5% induction and 3% maintenance doses of isoflurane gas. The uterine horns were removed, and animals were humanely euthanized according to IACUC approved protocols. During this step maternal whole blood was collected from the thoracic cavity after heart removal. The right and left uterine horns were further dissected to harvest right and left ovarian and uterine samples. Placentas at the ovary, middle, and cervical sections of the right and left uterine horns were quartered. One quarter of each placenta was further dissected to separate the maternal (decidua/junctional zone) and fetal (labyrinth) zones. Umbilical cord, liver, heart, and whole blood were collected from fetuses in the middle position of each uterine horn. Fetal sex was recorded by testes or uterine horn visualization. Maternal tissues sampled for collection were the lungs (caudal lobe), thoracic aorta, apex of the heart, liver, kidney cortex, spleen, and pancreas. Tissue samples were subsectioned to <0.2 g and were snap frozen in liquid nitrogen and stored at −80 °C until further processing.

### 2.5. Inductively Coupled Plasma Mass Spectrometry (ICP-MS)

Ti concentrations in tissue and blood samples were quantified using ICP-MS analysis. Tissue and blood samples were snap frozen in liquid nitrogen and later transferred to Teflon vials (Savillex). To each sample weighing over 0.15 g, 1 mL of concentrated $HNO_3$ was added. Samples weighing below 0.15 g received 0.5 mL of concentrated $HNO_3$. Samples were then sonicated for 1 h and subsequently set on a hot plate (110–130 °C) for at least 6 h. Once tissues were visibly dissolved, samples were cooled completely and vented by loosening the Teflon vial cap. Uncapped samples were placed on a hotplate encased a in polypropylene drying box to prevent contamination, to evaporate until about 95% of the acid had vaporized. Samples were then further digested with 1 mL of 8 N $HNO_3$ and 20 μL of HF and heated (120 °C) on the hotplate for 3 h, to ensure $TiO_2$ was dissolved. For dilution and transfer, condensate was collected with the rest of the sample by rolling the liquid along Teflon vial walls and pouring the total sample into metal-free polypropylene centrifuge tubes. Samples were diluted with MilliQ water to produce an acid concentration of 5% $HNO_3$ and 0.1% HF ready for ICP-MS analysis.

Ti concentrations in digested samples were quantified using a Nu AttoM high resolution ICP-MS, at medium resolution (3000) to remove interferences. The operating conditions were as follows: RF power of 1524 W, carrier gas flow of 1.00 L/min Ar, and nebulizer gas flow of ~36 psi Ar. Three replicates of masses $^{47}$Ti and $^{49}$Ti were measured in deflector scan mode with 100 ms peak dwell time, 100 sweeps/cycle, and averaged (RSD <5%). Calibration standards were prepared daily with Ti concentrations ranging from 0.01 to 10 ppb, in 5% $HNO_3$, with an instrument detection limit <0.10 ppb Ti, and a method detection limit of 10 ppb. Sample concentrations were determined using a linear regression through at least five standards, with a correlation coefficient >0.999 for all runs. Procedural blanks were prepared with each batch of samples following the same protocol, with average blank contribution of 0.29 ppb. Final concentrations were blank corrected by subtracting the average blank concentration, corrected for dilution volume of the sample. Quality control standard (PAS-28) were repeatedly measured after every sixth sample to account for instrument drift and monitor

reproducibility and reproduced with RSD <5% (n = 24).

### 2.6. Transmission electron microscopy imaging

Placental units (i.e., uterine artery segment, entire arcuate and radial network connecting to the uterine myometrium and placenta, and umbilical cord) were harvested at necropsy from the middle section of the right uterine horn. The placentas were rinsed and then submerged in cold (4 °C) phosphate buffered saline and cannulated by the uterine and umbilical artery with 4-inch steel blunt tip needles. A physiological saline solution (130 mM NaCl, 4.7 mM KCl, 1.18 mM $KH_2PO_4$, 1.17 mM $MgSO_4$ $7H_2O$, 1.6 mM $CaCl_2$, 14.9 mM $NaHCO_3$, 0.026 mM EDTA, and 5.5 mM glucose) was used to flush tissue of blood for 20 min or until tissue appeared devoid of blood at 80 μL/min using 50 mL syringe perfusion pump. The tissue was then perfused with a 2.5% glutaraldehyde, 4% paraformaldehyde fixative solution at 80 μL/min for 20 min. After fixation the uterine muscle was peeled away, and a 1 mm punch biopsy tool was used to sample the center of the placenta. The biopsy samples spanned from the decidua, through the junctional and labyrinth zones and ended at the chorionic plate. The biopsied tissue was immediately drop fixed into a glass vial containing 4 mL of 2.5% glutaraldehyde and 4% paraformaldehyde fixative solution and stored at 20 °C until further processing. Samples were subsequently dehydrated in a graded series of acetone and embedded in Embed812 resin. Sections 90 nm thin were cut on a Leica UC6 ultramicrotome and stained with saturated solution of uranyl acetate and lead citrate. Images were captured with an AMT (Advanced Microscopy Techniques) XR111 digital camera at 80Kv on a Philips CM12 transmission electron microscope.

### 2.7. Data presentation and Statistics

All organ data except for placenta is presented as one tissue per dam. For placenta, data is presented as a per dam average of 3 placentas from the right uterine horn and 3 placentas from the left uterine horn for the 6 dams evaluated in the study. For the fetal tissues, 2 representative fetus were evaluated for each dam. Fetus were taken from the middle of the right and left uterine horns as identified. For all ICP-MS data, values that were one or more order of magnitude above the mean for that tissue group were considered technical outliers and removed. To determine the appropriate statistical test for comparison between exposure groups for each tissue type a Shapiro-Wilk normality test was performed. This test assesses whether a data set is well-represented by a normal Gaussian distribution, and that there is an equal probability of each value to fall above or below the mean value of the data set. Data where both groups passed the normality test ($p > 0.05$) were assessed by Student's t-test. Data where at least one group did not pass the normality test ($p < 0.5$) were assessed by Mann-Whitney *U* test. Alpha was set to 0.05 for both tests. Right and left sides of the reproductive tract are presented and analyzed by Two-way ANOVA with Sidak's multiple comparisons test. Data is displayed as mean ± standard error of the mean (SEM). Samples that were below ICP-MS detectable limits were conservatively replaced by numerical values of the instrument's limit of detection.

## 3. Results

### 3.1. Maternal lung deposition of NPs

The total, daily, and additive lung deposition of NPs were calculated for each experimental group (Table 1). After considering daily deposition and clearance from repeated exposures, the total lung deposition for the nano-$TiO_2$ group was calculated to be 194.81 ± 1.89 μg.

### 3.2. Distribution of Ti to maternal, placental, and fetal tissues

The distribution of Ti was quantified in both exposed and control tissues (Fig. 2). Background Ti concentrations in the control group are consistent with previous literature evaluating nano-$TiO_2$ biodistribution [7,32]. Upon further investigation, it was found the maternal rodent diet was likely to be a source of Ti. A set of 3 Purina chow pellets were subjected to the same sample digestion protocol and using ICP-MS an average of 12,606.0 ± 6359.5 ppb of Ti was measured. Therefore, all animals were also exposed to Ti through oral ingestion.

In the inhalation exposure group, the Ti quantified in maternal lung tissue was 232,404.8 ± 18,223.3 ppb indicating successful pulmonary exposure utilizing the whole-body aerosol chamber (Fig. 2a). The right uterine horn and ovary from nano-$TiO_2$ exposed dams had significantly more Ti detected compared to the filtered air control dams (Fig. 2b). Regarding fetal tissues, the right umbilical cord and left fetal heart had significant higher and elevated Ti accumulation, respectively, in the nano-$TiO_2$ exposed group when compared to control (Fig. 2c).

Maternal, uteroplacental, and fetal organs were ranked by expected relative distribution in a pregnancy model based on previous work in a non-pregnant model [7] and considering the physiological changes during pregnancy [13]. The expected and actual relative amounts of Ti from highest to lowest in the exposed group is presented in Table 2. These values are presented as a percent of total ppb and corresponding Ti concentration in ppb. Furthermore, the distribution percentage to tissues outside of the lung in rank order (highest to lowest) after inhalation exposure as compared to controls are presented (Fig. 3). Maternal and fetal hearts accounted for over 35% of Ti translocation in controls, whereas most of the Ti (i.e., 19.24%) was identified in the maternal liver after gestational inhalation of nano-$TiO_2$ aerosols.

### 3.3. Distribution of Ti by placental zone, uterine position, and fetal sex

Ti concentrations were analyzed by uterine and placental anatomical position as well as by fetal sex (Fig. 4). In exposed animals there was on average 40.6 ± 7.2 ppb measured on the maternal side (decidua/junctional zone) of the placenta and 36.3 ± 11.1 ppb quantified on the fetal side (labyrinth) indicating no preferential placental zone for Ti accumulation (Fig. 4A). Similarly, there was no difference in the Ti amount detected in the either maternal or fetal placental zone for the filtered air group. There were no overall differences in the amount of Ti detected in the right vs. left uterine horn of either control or exposed groups (Fig. 4B). There were also no significant differences in Ti deposition pertaining to fetal sex in either control or exposed groups.

### 3.4. Intracellular localization of nanoparticles

NP agglomerates were visualized in 0 out of 4 filtered air placentas and 4 out of 4 nano-$TiO_2$ exposed placentas (Fig. 5). 3,000x magnification demonstrates NP agglomerates within the syncytium inside of the nucleus, rough endoplasmic reticulum, and intracellular vesicles (Fig. 5A and 5B). 3,800x shows microvilli extending into maternal sinus and presence of NP agglomerates within the cell in nano-$TiO_2$ exposed dams. Agglomerates are embedded in rough endoplasmic reticulum and vesicles near the plasma membrane surface (Fig. 5C and 5D). 10,000x magnification shows high magnification of space between cells and that NP agglomerates are present within confines of cell membrane from exposed placentas and are near rough endoplasmic reticulum and plasma membrane vesicles (Fig. 5E and 5F).

## 4. Discussion

This study aimed to examine the systemic distribution of inhaled nano-$TiO_2$ aerosols during pregnancy. Previous work has identified links between inhalation exposure and perturbations to pregnancy health (e.g., miscarriage, FGR) [9,10], with a particular emphasis on the placenta and its role as a protective barrier for the fetus. We found evidence in support of NP translocation to secondary maternal organs, the placenta, and fetal tissues after maternal inhalation. Furthermore, Ti was

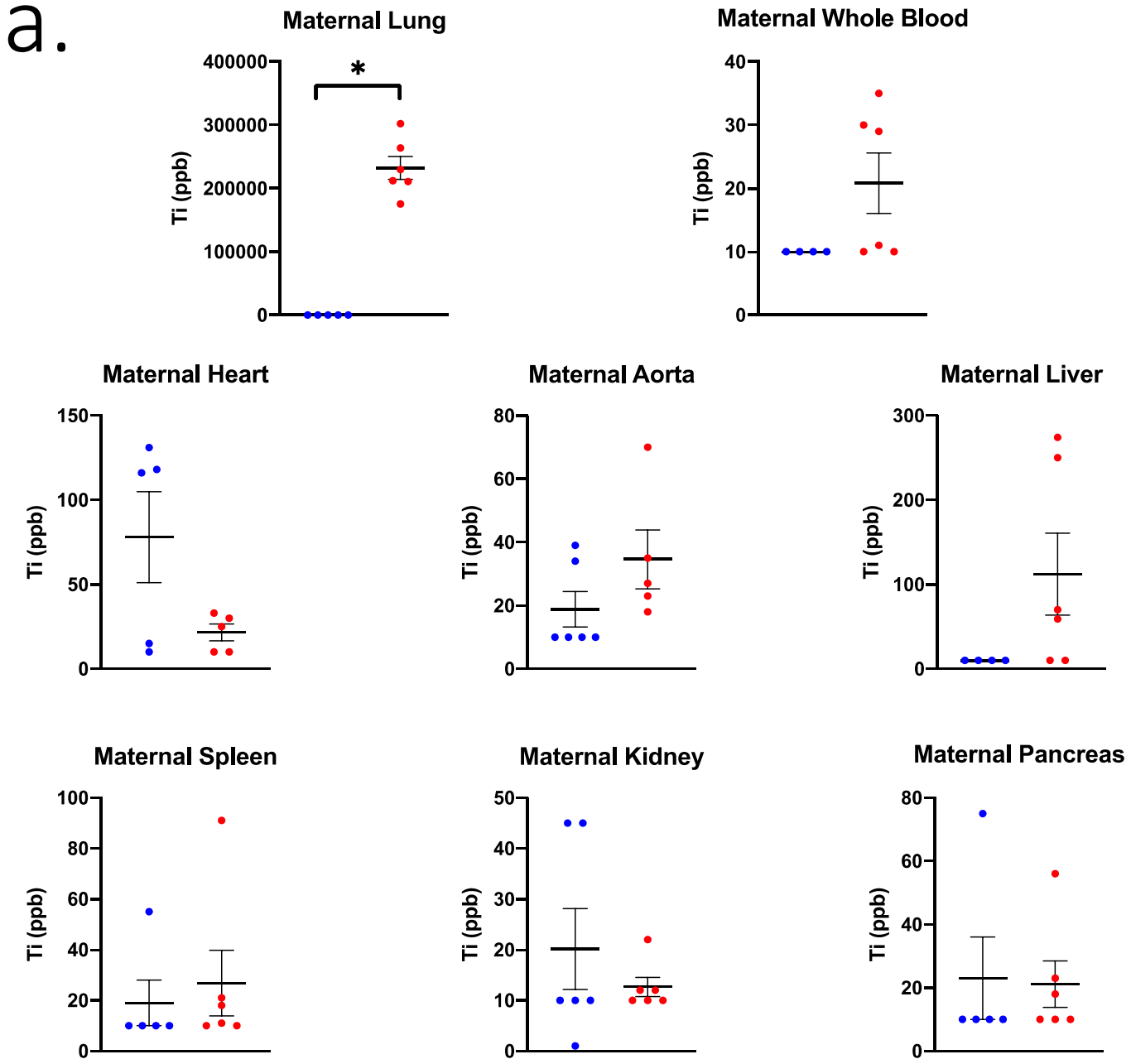


**Fig. 2.** Ti concentrations in ppb measured in **(A)** maternal, **(B)** uteroplacental, and **(C)** fetal tissues on GD 20 using ICP-MS analysis. Limit of Detection = 10 ppb. n = 6 dams per group. Analysis by Student's t-test or Mann-Whitney *U* test depending on distribution, mean ± SEM reported. * = $p \leq 0.05$, T = $\leq 0.07$.

identified in the decidua/junctional zone and labyrinth zone of the placenta. This accumulation did not differ based on intrauterine position or fetal sex.

These results support previous findings that inhaled nano-$TiO_2$ translocate and deposit in tissues secondary from the lung. Pujalte et al. found detectable Ti in the blood, lymph nodes, liver, kidneys, and spleen in male Sprague Dawley rats within 3 h after a single inhalation exposure of 20 nm nano-$TiO_2$ [7]. In another study using a male rat model, Ti persisted in the liver and spleen up to 180 days after exposure cessation [33]. While our study did not include a time course or recovery period component, it contributes to the body of evidence that inhaled NP aerosols exit the lung, systemically distribute, and deposit in distal organs.

During pregnancy the placenta acts to function as a protective barrier to prevent harmful substance(s) from transferring to the fetus. Evidence from *in vitro* [34], *ex vivo* [9,35,36], and *in vivo* [9] studies conclude that NPs can translocate across the placenta and access the fetal compartment [37]. Previous studies have detected nano-$TiO_2$ within placental and fetal tissue [32,38,39] after oral or intravenous exposure. Silver NPs (e.g., 18–20 nm) have been identified within maternal tissues, placentas, and fetuses via TEM imaging coupled with single particle ICP-MS after repeated exposure to nano-silver aerosols [40]. Using optical imaging and dark-field microscopy, our laboratory recently identified the deposition and transfer of nanosized polystyrene particles within maternal, placental, and fetal tissues after maternal pulmonary exposure in late pregnancy [9]. Others have also evaluated fluorescently-labeled NP deposition by placental zone and found partial deposition in the chorionic plate, but without consideration for other variables such as

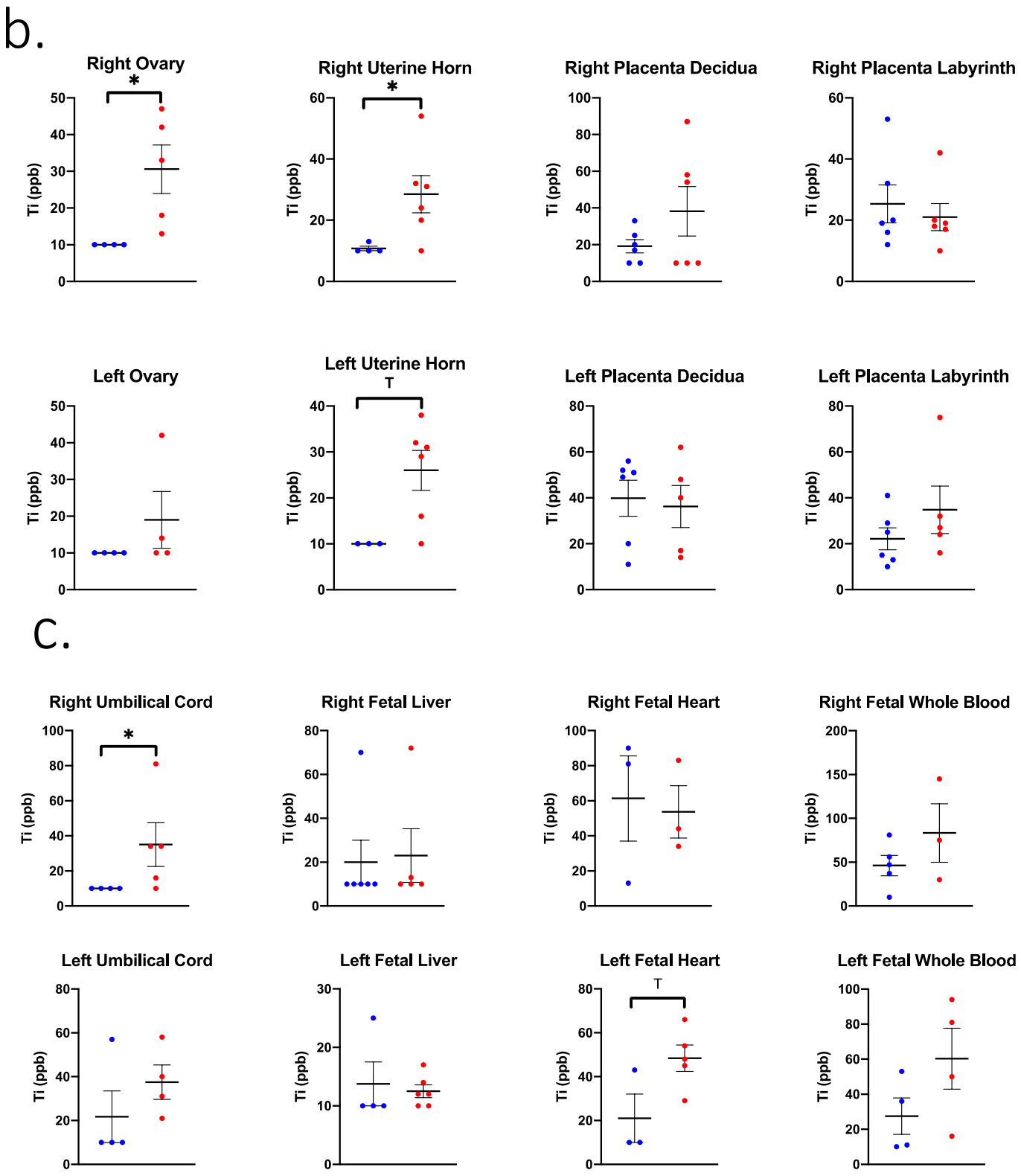


**Fig. 2.** (*continued*).

intrauterine location or fetal sex [41]. Significance evidence supports the conclusion that the placenta is an imperfect barrier and may be permeated by nanosized xenobiotic particles, allowing NP translocation to the fetus. Unfortunately, the mechanisms permitting NP transport across the placenta and the ramifications for progeny health remain unknown.

Using a toxicological approach and a pharmacologic absorption, distribution, metabolism, and excretion (ADME) model, we evaluated likely organ distribution in a pregnancy after inhalation exposure. We then calculated the percent deposition of Ti within the maternal lung and extrapulmonary tissues (Table 2). This information may inform future study determination of the appropriate *in vitro* dosing based on

**Table 2**
Rank order of organs with expected highest to lowest relative percent Ti concentrations and actual concentrations (excluding lung). Data presented as a percent of the total of average Ti measured in nano-$TiO_2$ exposed.

| Organ | Expected exposure order (highest to lowest Ti concentration) | Actual exposure order (highest to lowest Ti concentration) | Actual % of nano-$TiO_2$ | Corresponding Ti (ppb) |
|---|---|---|---|---|
| Maternal Liver | 1 | 1 | 19.24 | 104.39 |
| Maternal Kidney | 2 | 15 | 2.33 | 12.67 |
| Uterus | 3 | 9 | 5.02 | 27.25 |
| Placenta Decidua | 4 | 4 | 6.87 | 37.27 |
| Placenta Labyrinth | 5 | 8 | 5.03 | 27.27 |
| Maternal Spleen | 6 | 10 | 4.95 | 26.83 |
| Maternal Aorta | 7 | 6 | 6.39 | 34.66 |
| Maternal Whole Blood | 8 | 13 | 3.84 | 20.83 |
| Maternal Heart | 9 | 7 | 5.87 | 31.84 |
| Maternal Pancreas | 10 | 12 | 3.90 | 21.12 |
| Ovaries | 11 | 11 | 4.69 | 25.44 |
| Umbilicals | 12 | 5 | 6.65 | 36.10 |
| Fetal Liver | 13 | 14 | 3.02 | 16.36 |
| Fetal Whole Blood | 14 | 2 | 12.93 | 70.14 |
| Fetal Heart | 15 | 3 | 9.28 | 50.38 |
| Total Ti (ppb) | | | | 542.59 |

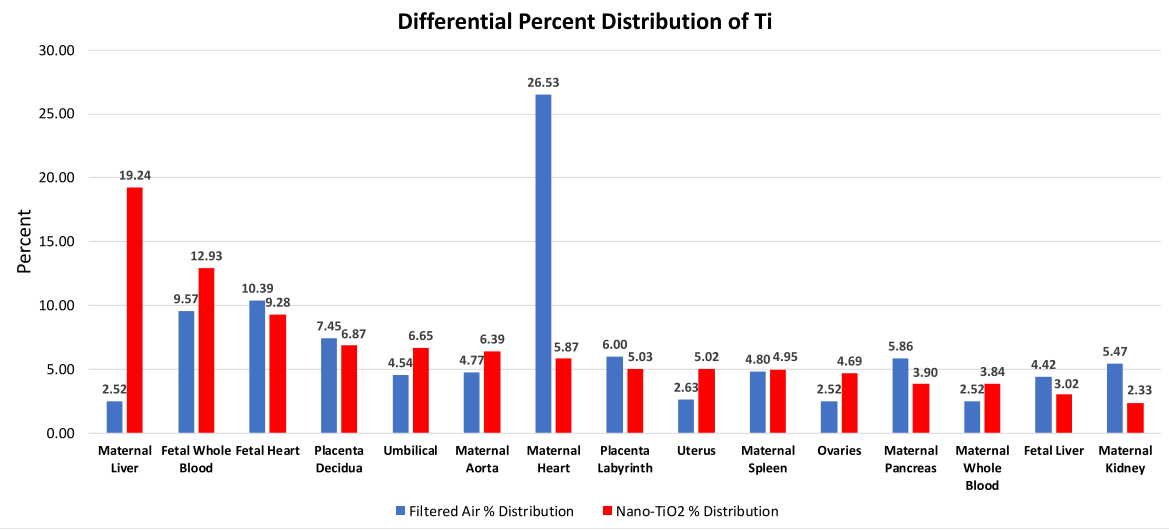


**Fig. 3.** Differential Ti tissue distribution outside of the lung in control and nano-$TiO_2$ exposed groups. Data is displayed as percent of total Ti excluding the maternal lung in each group.

percent of material translocated after pulmonary inhalation exposure.

The samples derived from our control filtered air exposures also had detectable Ti using ICP-MS analyses. This Ti likely originated from the rodent chow; thus, representing an ingestion exposure in both control and inhalation exposure groups. Therefore, the data presented here describes anatomical accumulation of Ti after oral exposure or after combination of inhalation and ingestion exposures. This allows for the differential analysis of Ti deposition after oral or pulmonary exposure separate from the original site of exposure (Fig. 3). In the control group (oral ingestion only), nearly 50% of all Ti was identified in the maternal, fetal heart, and fetal whole blood tissue (i.e., 26.53%, 10.39%, and 9.57% respectively), followed by the placenta decidua and placenta labyrinth. These outcomes indicate important sites of Ti accumulation with dietary exposures. Unfortunately, intestinal concentrations were not evaluated within the confines of this study. Unsurprisingly, maternal lung accounted for 99.4% of all quantified Ti after inhalation exposure; however, of the remaining translocated Ti, 19.24%% was identified in maternal liver, followed by fetal whole blood, fetal heart, and placental decidua (i.e., 12.93%, 9.28%, and 6.87%, respectively) (Fig. 3). This information suggests there is differential distribution of Ti after oral or pulmonary $TiO_2$ exposure. Importantly, fetal whole blood and fetal hearts accumulate nearly 20% of Ti accumulation in both oral and pulmonary exposure scenarios. This may be associated with increased uteroplacental blood flow during pregnancy, an inability for placental Ti efflux, and/or a fetal Ti accumulation. Future investigations should further examine inhalation and ingestion NP administration and compare the distribution profiles.

There is strong evidence to suggest that adverse placental outcomes affecting pregnancy can be influenced by intrauterine positioning [26] and fetal sex [42]. Our previous work investigated maternal nano-$TiO_2$ inhalation and fetal growth restriction and found reductions in fetal weight on GD 20 dependent on uterine horn (i.e. right vs. left), position within that horn (i.e. ovary end, middle, or cervical end), and timing of maternal exposure [11]. We had originally theorized that nano-$TiO_2$ translocation and accumulation may influence these growth disparities; however, there were no significant differences in uteroplacental Ti deposition in this study (Fig. 4). Fetal sex was assessed due to the role it plays in nutrient uptake by the placenta [43]. It has been theorized that male fetuses exert higher demand for nutrient uptake from the mother for maximal growth and thus receive more blood flow [44]; subsequently, increased perfusion to male fetuses may result in greater particle deposition. Our findings revealed no significant difference in Ti

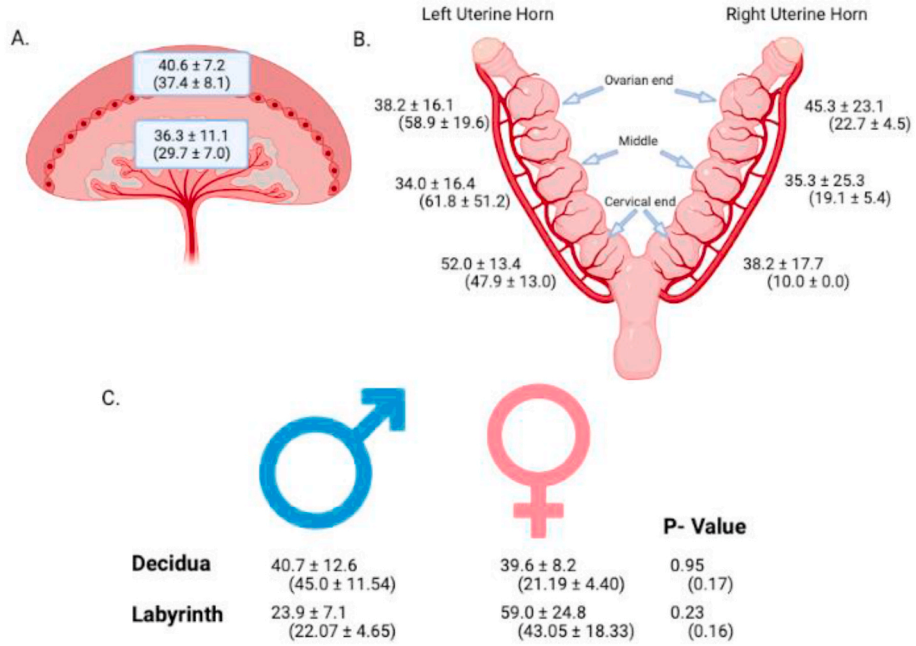


**Fig. 4.** Placental accumulation of Ti (ppb) measured by ICP-MS analysis from nano-$TiO_2$ and filtered air exposed dams. **A.** Mean ± SEM values of Ti in ppb measured in the maternal zone (decidua/junctional zone) and fetal zone (labyrinth) of all exposed placentas. **B.** Mean ± SEM values of Ti in ppb measured in exposed placentas from left and right horns in ovarian end, middle, and cervical end locations. **C.** Mean ± SEM values of Ti in ppb measured in male and female placentas. Data are presented as exposed means ± SEM and (control means ± SEM). n = 6 dams. Analysis by Student's t-test, mean ± SEM reported. Images created with BioRender.com.

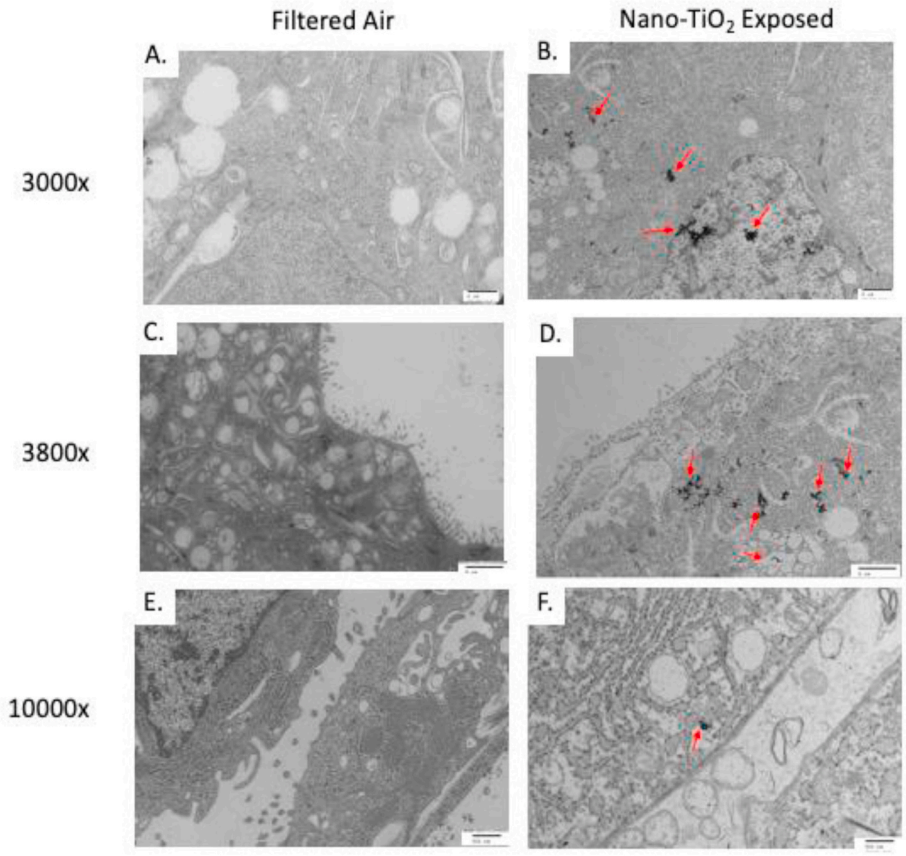


**Fig. 5.** Transmission Electron Microscopy (TEM) image of particle distribution in the trophoblasts in the labyrinth zone of the placenta. Representative images (**A-D** scale bar 2 μm, **E** and **F** scale bar 500 nm). Particles were visualized in 0 of 4 filtered air placentas and 4 of 4 nano-$TiO_2$ exposed placentas. All placentas were harvested from the middle section of the right uterine horn.

accumulation based on fetal sex. Together, these results show accumulation of Ti regardless of intrauterine location, placental zone, or fetal sex after maternal repeated inhalation exposure.

There are some limitations associated with this study. First, the ingestion exposure to Ti was an unintended confounding factor for the Ti measurements in the nano-$TiO_2$ exposed group. As mentioned above, this likely originated from the rodent chow diet. Future studies may obtain Ti-free animal feed to remove any background contribution of

elemental Ti for analysis. ICP-MS is unable to differentiate between elemental Ti and nano-$TiO_2$ NPs after the digestion protocol. Therefore, it is unknown whether the Ti measured from the tissues and rodent diet were in particulate or metal element contaminant form [45]. However, titanium dioxide is known to be a commercial food additive or colorant, therefore this outcome is further evidence of its widespread use and application [46]. Additionally, the exposure period spanned from pre-implantation (GD 4) up to 24–48 h prior to delivery (GD 19) and did not include sub-groups of animals to gather time course data of NP distribution. Future studies may include this analysis to provide snapshots of tissue Ti content at each trimester, allowing for assessments of distribution throughout critical windows of gestation. This accumulation is also measure only at GD 20; it is unclear if the concentrations identified at this timepoint are transient or continue to the postnatal period. Lastly, we deduce that the visualized NPs within the syncytium of exposed dams using TEM are nano-$TiO_2$. However, this should be confirmed in future studies by using Scanning Electron Microscopy, Energy Dispersive X-Ray Analysis (SEM-EDX) and through co-localization staining to identify the intracellular location.

Overall, this study evaluated the systemic distribution of Ti after NP aerosol inhalation in a pregnancy model. The results from this study infer that secondary tissues, including the placenta and fetus, are vulnerable to direct NP interaction(s) after maternal inhalation during pregnancy. Given the many critical roles the placenta plays during pregnancy to guard fetal development, further research to investigate how placental NP aerosol exposure and deposition may impact placental function are warranted.

## Funding sources

This work was supported by the National Institutes of Health [R01-ES031285; R00-ES27483; P30-ES005022; T32-ES007148; R25-ES020721], ASPET-SURF, and RISE at Rutgers.

## Declaration of competing interest

None.

## Acknowledgments

We would like to acknowledge Ms. Chelsea Cary for assisting with necropsy tissue and data collections, and for her time in collaboration with Ms. Talia Seymore for the thoughtful review of this manuscript. We would like to thank Mr. Rajesh Patel from the Core Imaging Lab in the Department of Pathology in the Robert Wood Johnson Medical Center for the processing, sectioning, and embedding of the TEM slides and for guidance on TEM microscope usage. We would also like to thank Dr. Kenneth Reuhl for aiding in the interpretation of TEM micrographs.

## References

[1] G. Bachler, et al., Translocation of gold nanoparticles across the lung epithelial tissue barrier: combining in vitro and in silico methods to substitute in vivo experiments, Part. Fibre Toxicol. 12 (2015), 18-18.
[2] F. Fazlollahi, et al., Nanoparticle translocation across mouse alveolar epithelial cell monolayers: species-specific mechanisms, Nanomed. Nanotechnol. Biol. Med. 9 (6) (2013) 786–794.
[3] A. Elder, et al., Translocation of inhaled ultrafine manganese oxide particles to the central nervous system, Environ. Health Perspect. 114 (8) (2006) 1172–1178.
[4] A.J. Cohen, et al., Estimates and 25-year trends of the global burden of disease attributable to ambient air pollution: an analysis of data from the Global Burden of Diseases Study 2015, Lancet (London, England) 389 (10082) (2017) 1907–1918.
[5] M.R. Miller, et al., Inhaled nanoparticles accumulate at sites of vascular disease, ACS Nano 11 (5) (2017) 4542–4552.
[6] A. Nemmar, et al., Passage of inhaled particles into the blood circulation in humans, Circulation 105 (4) (2002) 411–414.
[7] I. Pujalté, et al., Toxicokinetics of titanium dioxide (TiO(2)) nanoparticles after inhalation in rats, Toxicol. Lett. 265 (2017) 77–85.
[8] C. Schleh, et al., Biodistribution of inhaled gold nanoparticles in mice and the influence of surfactant protein, J. Aerosol Med. Pulm. Drug Deliv. 25 (1) (2013) 24–30.
[9] S.B. Fournier, et al., Nanopolystyrene translocation and fetal deposition after acute lung exposure during late-stage pregnancy, Part. Fibre Toxicol. 17 (1) (2020) 55.
[10] L. Campagnolo, et al., Silver nanoparticles inhaled during pregnancy reach and affect the placenta and the foetus, Nanotoxicology 11 (5) (2017) 687–698.
[11] J.N. D'Errico, S.B. Fournier, P.A. Stapleton, Considering intrauterine location in a model of fetal growth restriction after maternal titanium dioxide nanoparticle inhalation, Front.Toxicol. 3 (11) (2021).
[12] N.M. Liu, et al., Evidence for the presence of air pollution nanoparticles in placental tissue cells, Sci. Total Environ. 751 (2021) 142235.
[13] P. Soma-Pillay, et al., Physiological changes in pregnancy, Cardiovasc. J. Afr. 27 (2) (2016) 89–94.
[14] A. Nakai, et al., Assessment of the hepatic arterial and portal venous blood flows during pregnancy with Doppler ultrasonography, Arch. Gynecol. Obstet. 266 (1) (2002) 25–29.
[15] W. Dunlop, Serial changes in renal haemodynamics during normal human pregnancy, Br. J. Obstet. Gynaecol. 88 (1) (1981) 1–9.
[16] L. Aengenheister, et al., Investigating the accumulation and translocation of titanium dioxide nanoparticles with different surface modifications in static and dynamic human placental transfer models, Eur. J. Pharm. Biopharm. 142 (2019) 488–497.
[17] Y. Zhang, et al., Titanium dioxide nanoparticles induce proteostasis disruption and autophagy in human trophoblast cells, Chem. Biol. Interact. 296 (2018) 124–133.
[18] H. Zhong, et al., Maternal exposure to CeO(2)NPs during early pregnancy impairs pregnancy by inducing placental abnormalities, J. Hazard Mater. 389 (2020) 121830.
[19] A.B. Abukabda, et al., Maternal titanium dioxide nanomaterial inhalation exposure compromises placental hemodynamics, Toxicol. Appl. Pharmacol. 367 (2019) 51–61.
[20] E.C. Bowdridge, et al., Maternal engineered nanomaterial inhalation during gestation disrupts vascular kisspeptin reactivity, Toxicol. Sci. 169 (2) (2019) 524–533.
[21] C. Teng, et al., Oral Co-Exposures to zinc oxide nanoparticles and CdCl(2) induced maternal-fetal pollutant transfer and embryotoxicity by damaging placental barriers, Ecotoxicol. Environ. Saf. 189 (2020) 109956.
[22] M. Nedder, et al., Uptake of cerium dioxide nanoparticles and impact on viability, differentiation and functions of primary trophoblast cells from human placenta, Nanomaterials 10 (7) (2020) 1309.
[23] T. Wainstock, et al., Fetal sex modifies effects of prenatal stress exposure and adverse birth outcomes, Stress 18 (1) (2015) 49–56.
[24] J. Challis, et al., Fetal sex and preterm birth, Placenta 34 (2) (2013) 95–99.
[25] X. Li, et al., A pilot study of mothers and infants reveals fetal sex differences in the placental transfer efficiency of heavy metals, Ecotoxicol. Environ. Saf. 186 (2019) 109755.
[26] S. Zia, Placental location and pregnancy outcome, J. Turk. Ger. Gynecol. Assoc. 14 (4) (2013) 190–193.
[27] P.A. Stapleton, et al., Maternal engineered nanomaterial exposure and fetal microvascular function: does the Barker hypothesis apply? Am. J. Obstet. Gynecol. 209 (3) (2013) 227, e1-11.
[28] S.B. Fournier, et al., Effect of gestational age on maternofetal vascular function following single maternal engineered nanoparticle exposure, Cardiovasc. Toxicol. 19 (4) (2019) 321–333.
[29] J. Yi, et al., Whole-body nanoparticle aerosol inhalation exposures, J Vis Exp (75) (2013) e50263-e50263.
[30] X. Zhang, et al., Maternal PM2.5 exposure triggers preterm birth: a cross-sectional study in Wuhan, China, Global Health Research and Policy 5 (1) (2020) 17.
[31] P.A. Stapleton, et al., Uterine microvascular sensitivity to nanomaterial inhalation: an in vivo assessment, Toxicol. Appl. Pharmacol. 288 (3) (2015) 420–428.
[32] J. Lee, et al., Titanium dioxide nanoparticles oral exposure to pregnant rats and its distribution, Part. Fibre Toxicol. 16 (1) (2019) 31.
[33] L. Gate, et al., Biopersistence and translocation to extrapulmonary organs of titanium dioxide nanoparticles after subacute inhalation exposure to aerosol in adult and elderly rats, Toxicol. Lett. 265 (2017) 61–69.
[34] L. Aengenheister, et al., Gold nanoparticle distribution in advanced in vitro and ex vivo human placental barrier models, J. Nanobiotechnol. 16 (1) (2018) 79.
[35] J.N. D'Errico, S.B. Fournier, P.A. Stapleton, Ex vivo perfusion of the rodent placenta, J Vis Exp 147 (2019), https://doi.org/10.3791/59412.
[36] J.N. D'Errico, et al., Identification and quantification of gold engineered nanomaterials and impaired fluid transfer across the rat placenta via ex vivo perfusion, Biomed. Pharmacother. 117 (2019) 109148.
[37] E. Bongaerts, et al., Translocation of (ultra)fine particles and nanoparticles across the placenta; a systematic review on the evidence of in vitro, ex vivo, and in vivo studies, Part. Fibre Toxicol. 17 (1) (2020) 56.
[38] K. Yamashita, et al., Silica and titanium dioxide nanoparticles cause pregnancy complications in mice, Nat. Nanotechnol. 6 (5) (2011) 321–328.
[39] F. Hong, et al., Maternal exposure to nanosized titanium dioxide suppresses embryonic development in mice, Int. J. Nanomed. 12 (2017) 6197–6204.
[40] L. Campagnolo, et al., Silver nanoparticles inhaled during pregnancy reach and affect the placenta and the foetus, Nanotoxicology 11 (5) (2017) 687–698.
[41] D. Ho, et al., Maternal-placental-fetal biodistribution of multimodal polymeric nanoparticles in a pregnant rat model in mid and late gestation, Sci. Rep. 7 (1) (2017), 2866-2866.
[42] C.S. Rosenfeld, Sex-specific placental responses in fetal development, Endocrinology 156 (10) (2015) 3422–3434.

[43] M. Saoi, et al., Placental metabolomics for assessment of sex-specific differences in fetal development during normal gestation, Sci. Rep. 10 (1) (2020) 9399.
[44] P. Alur, Sex differences in nutrition, growth, and metabolism in preterm infants, Front Pediatr 7 (2019) 22.
[45] H.-T. Kim, et al., Evaluation of arsenic, cadmium, lead and mercury contamination in over-the-counter available dry dog foods with different animal ingredients (red meat, poultry, and fish), Frontiers in veterinary science 5 (2018), 264-264.
[46] V Bampidis, et al., European Food Safety Authority, Safety and efficacy of a feed additive consisting of titanium dioxide for all animal species, EFSA J 19 (6) (2021), 6630, https://doi.org/10.2903/j.efsa.2021.6630.